PHYSICAL REVIEW D **93,** 035004 (2016)

Automatic predictions in the Georgi-Machacek model at next-to-leading order accuracy

Céline Degrande,[1,*] Katy Hartling,[2,†] Heather E. Logan,[2,‡] Andrea D. Peterson,[2,§] and Marco Zaro[3,4,‖]

[1]*Institute for Particle Physics Phenomenology, Department of Physics, Durham University, Durham DH1 3LE, United Kingdom*

[2]*Ottawa-Carleton Institute for Physics, Carleton University, 1125 Colonel By Drive, Ottawa, Ontario K1S 5B6, Canada*

[3]*Sorbonne Universités, UPMC Univ. Paris 06, UMR 7589, LPTHE, F-75005 Paris, France*

[4]*CNRS, UMR 7589, LPTHE, F-75005 Paris, France*

(Received 17 December 2015; published 4 February 2016)

We study the phenomenology of the Georgi-Machacek model at next-to-leading order in QCD matched to a parton shower, using a fully automated tool chain based on MadGraph5_aMC@NLO and FeynRules. We focus on the production of the fermiophobic custodial fiveplet scalars H_5^0, $H_5^\pm$, and $H_5^{\pm\pm}$ through vector boson fusion (VBF), associated production with a vector boson (VH_5), and scalar pair production (H_5H_5). For these production mechanisms we compute next-to-leading order corrections to production rates as well as to differential distributions. Our results demonstrate that the Standard Model overall K-factors for such processes cannot in general be directly applied to beyond-the-Standard-Model distributions, due both to differences in the scalar electroweak charges and to the variation of the K-factors over the differential distributions.

DOI: 10.1103/PhysRevD.93.035004

I. INTRODUCTION

A deeper understanding of the scalar sector is a primary objective of the CERN LHC. In addition to precisely measuring the 125 GeV Higgs boson, Run II of the LHC will dedicate its efforts to searching for signs of additional Higgs particles, which arise in a number of beyond-the-Standard-Model (BSM) scenarios. One such scenario is the Georgi-Machacek (GM) model [1,2], which extends the Standard Model (SM) with two scalar isospin triplets in a way that preserves the SM value of $\rho = M_W^2/M_Z^2\cos^2\theta_W = 1$ at tree level. The phenomenology of the GM model has previously been studied in Refs. [3–28], including the application of a variety of constraints upon the model parameter space. It has been shown to possess a decoupling limit and can thus accommodate a SM-like 125 GeV boson [21]. Furthermore, the tree-level couplings of this SM-like Higgs to fermions and vector bosons may be enhanced in comparison to the SM [25], a feature that cannot be accommodated in models that contain only scalars in $SU(2)$ singlet or doublet representations. The GM model can also be embedded in more elaborate theoretical scenarios, such as little Higgs [29,30] and supersymmetric [31–33] models, or generalized to larger $SU(2)$ multiplets [34].

The Georgi-Machacek model provides a useful benchmark framework for BSM Higgs searches. In addition to an SM-like scalar singlet h, the GM model also contains an extra scalar singlet H, a triplet H_3, and a fiveplet H_5 under the custodial symmetry. The structure of the model with respect to the custodial singlet and triplet states is similar to that of the two Higgs doublet model (2HDM); as a result, the experimental searches and extensive analysis for 2HDM states can often be recast in terms of the GM singlet and triplet scalars [25]. It is therefore particularly interesting to focus on the custodial fiveplet states, H_5^0, $H_5^\pm$, and $H_5^{\pm\pm}$. These scalars are fermiophobic and couple preferentially to vector bosons. As a result, the GM fiveplet contains two features that are absent from both the SM and the 2HDM: a doubly charged scalar $H_5^{\pm\pm}$ and charged scalar states that couple to vector bosons. Consequently, the fermiophobic fiveplet states are produced primarily through the vector boson fusion (VBF) and associated production (VH_5) modes. This is in contrast to the 2HDM, where the heavy scalars are dominantly produced through associated production with a top quark or in top decays. These features lead to unique phenomenology and can be used to parametrize effects not captured by other common benchmark models.

For the Georgi-Machacek model to be truly useful as a LHC benchmark, efficient and accurate calculations must be accessible to both phenomenologists and experimentalists. Great strides have been made in reducing both theoretical and experimental uncertainties, making next-to-leading order (NLO) or higher order calculations standard practice. Therefore, we describe the use of a fully automated tool

*celine.degrande@durham.ac.uk
†khally@physics.carleton.ca
‡logan@physics.carleton.ca
§apeterso@physics.carleton.ca
‖zaro@lpthe.jussieu.fr

chain (which combines the FeynRules [35] and MadGraph5_aMC@NLO [36] frameworks with the calculator GMCALC [37]) to produce NLO differential distributions in the GM model, focusing on the examples of VBF, VH_5, and H_5H_5 production of the fiveplet states. In particular, we illustrate the insufficiency of extending the SM overall K-factors to BSM distributions, due to two factors. First, differential K-factors can vary substantially for certain distributions (particularly in the case of VBF). Second, the overall K-factors for differently charged states can be somewhat different. These considerations are important for accurately determining the effects of typical selection cuts, which is essential for measuring new states in the event of a discovery.

This paper is organized as follows. In the following section, we describe in more detail the scalar potential, spectrum, and couplings of the Georgi-Machacek model. In Sec. III, we then outline the tools used for our fully automated NLO calculations. Finally, in Secs. IV, V, and VI, we present cross sections, K-factors, and differential distributions for VBF, VH_5, and pair production (H_5H_5), respectively, of the fiveplet states. We conclude in Sec. VII. For completeness, some details of the scalar potential of the GM model are collected in an Appendix. The model files for the automated tool chain used to produce these results are publicly available on http://feynrules.irmp.ucl.ac.be/wiki/GeorgiMachacekModel.

II. MODEL

The scalar sector of the GM model [1,2] consists of the usual complex isospin doublet (ϕ^+, ϕ^0) with hypercharge[1] $Y = 1$, a real triplet (ξ^+, ξ^0, ξ^-) with $Y = 0$, and a complex triplet $(\chi^{++}, \chi^+, \chi^0)$ with $Y = 2$. The doublet is responsible for the fermion masses as in the SM.

The scalar potential is chosen by hand to preserve a global $SU(2)_L \times SU(2)_R$ symmetry. This ensures that $\rho = M_W^2/M_Z^2\cos^2\theta_W = 1$ at tree level, as required by precise experimental measurements [38]. In order to make the global $SU(2)_L \times SU(2)_R$ symmetry explicit, we write the doublet in the form of a bidoublet Φ and combine the triplets to form a bitriplet X:

$$\Phi = \begin{pmatrix} \phi^{0*} & \phi^+ \\ -\phi^{+*} & \phi^0 \end{pmatrix}, \qquad X = \begin{pmatrix} \chi^{0*} & \xi^+ & \chi^{++} \\ -\chi^{+*} & \xi^0 & \chi^+ \\ \chi^{++*} & -\xi^{+*} & \chi^0 \end{pmatrix}. \tag{1}$$

The vacuum expectation values (vevs) are defined by $\langle\Phi\rangle = \frac{v_\phi}{\sqrt{2}} I_{2\times 2}$ and $\langle X\rangle = v_\chi I_{3\times 3}$, where I is the unit matrix and the Fermi constant G_F fixes the combination of vevs,

$$v_\phi^2 + 8v_\chi^2 \equiv v^2 = \frac{1}{\sqrt{2}G_F} \approx (246\ \text{GeV})^2. \tag{2}$$

These vevs are parametrized in terms of a mixing angle θ_H according to

$$c_H \equiv \cos\theta_H = \frac{v_\phi}{v}, \qquad s_H \equiv \sin\theta_H = \frac{2\sqrt{2}v_\chi}{v}. \tag{3}$$

The quantity s_H^2 represents the fraction of the squared gauge boson masses M_W^2 and M_Z^2 that is generated by the vev of the triplets, while c_H^2 represents the fraction generated by the usual Higgs doublet. The most general scalar potential that preserves the custodial $SU(2)$ symmetry may be found in the Appendix.

After symmetry breaking, the physical fields can be organized by their transformation properties under the custodial $SU(2)$ symmetry into a fiveplet, a triplet, and two singlets. The fiveplet and triplet states are given by

$$\begin{aligned} H_5^{++} &= \chi^{++}, \qquad H_5^+ = \frac{(\chi^+ - \xi^+)}{\sqrt{2}}, \\ H_5^0 &= \sqrt{\frac{2}{3}}\xi^0 - \sqrt{\frac{1}{3}}\chi^{0,r}, \\ H_3^+ &= -s_H\phi^+ + c_H\frac{(\chi^+ + \xi^+)}{\sqrt{2}}, \\ H_3^0 &= -s_H\phi^{0,i} + c_H\chi^{0,i}, \end{aligned} \tag{4}$$

where we have decomposed the neutral fields into real and imaginary parts according to

$$\begin{aligned} \phi^0 &\to \frac{v_\phi}{\sqrt{2}} + \frac{\phi^{0,r} + i\phi^{0,i}}{\sqrt{2}}, \\ \chi^0 &\to v_\chi + \frac{\chi^{0,r} + i\chi^{0,i}}{\sqrt{2}}, \\ \xi^0 &\to v_\chi + \xi^0. \end{aligned} \tag{5}$$

The states of the custodial fiveplet $(H_5^{\pm\pm}, H_5^\pm, H_5^0)$ have a common mass m_5 and the states of the custodial triplet $(H_3^\pm, H_3^0)$ have a common mass m_3. Because the states in the custodial fiveplet contain no doublet field content, they do not couple to fermions (i.e. they are fermiophobic).

The two custodial singlets mix by an angle α, and the resulting mass eigenstates are given by

$$h = \cos\alpha\,\phi^{0,r} - \sin\alpha\,H_1^{0\prime}, \qquad H = \sin\alpha\,\phi^{0,r} + \cos\alpha\,H_1^{0\prime}, \tag{6}$$

where

$$H_1^{0\prime} = \sqrt{\frac{1}{3}}\xi^0 + \sqrt{\frac{2}{3}}\chi^{0,r}. \tag{7}$$

[1]We normalize the hypercharge operator such that $Q = T^3 + Y/2$.

We denote their masses by m_h and m_H. The singlet h is normally identified as the 125 GeV SM-like Higgs boson discovered at the LHC [39–41]. Formulas for the masses m_h, m_H, m_3, and m_5, as well as the mixing angle α, may be found in the Appendix.

The fiveplet states couple to vector bosons according to the following Feynman rules [8,21,42],

$$H_5^0 W_\mu^+ W_\nu^-: \sqrt{\frac{2}{3}} i g^2 v_\chi g_{\mu\nu} = 2(\sqrt{2}G_F)^{1/2} M_W^2 \left(-\frac{1}{\sqrt{3}} s_H\right)(-i g_{\mu\nu}), \quad (8)$$

$$H_5^0 Z_\mu Z_\nu: -\sqrt{\frac{8}{3}} i \frac{g^2}{c_W^2} v_\chi g_{\mu\nu} = 2(\sqrt{2}G_F)^{1/2} M_Z^2 \left(\frac{2}{\sqrt{3}} s_H\right)(-i g_{\mu\nu}), \quad (9)$$

$$H_5^+ W_\mu^- Z_\nu: -\sqrt{2} i \frac{g^2}{c_W} v_\chi g_{\mu\nu} = 2(\sqrt{2}G_F)^{1/2} M_W M_Z (s_H)(-i g_{\mu\nu}), \quad (10)$$

$$H_5^{++} W_\mu^- W_\nu^-: 2 i g^2 v_\chi g_{\mu\nu} = 2(\sqrt{2}G_F)^{1/2} M_W^2 (-\sqrt{2} s_H)(-i g_{\mu\nu}), \quad (11)$$

where we write the coupling in multiple forms to make contact with the notation of Refs. [8,43]. The triplet vev v_χ is called v' in Ref. [8], and the factors F_{VV} in Eq. (5.2) of Ref. [43] correspond in this model to

$$F_{W^+W^-} = -\frac{1}{\sqrt{3}} s_H \qquad (H_5^0 \text{ production}), \quad (12)$$

$$F_{ZZ} = \frac{2}{\sqrt{3}} s_H \qquad (H_5^0 \text{ production}), \quad (13)$$

$$F_{W^\pm Z} = s_H \qquad (H_5^\pm \text{ production}), \quad (14)$$

$$F_{W^\pm W^\pm} = -\sqrt{2} s_H \qquad (H_5^{\pm\pm} \text{ production}). \quad (15)$$

Note in particular that, for H_5^0, one cannot simply rescale the vector boson fusion cross section of the SM Higgs boson because the ratio of the WW and ZZ couplings is different than in the SM.

Additionally, two fiveplet scalars may also couple to a single vector boson through the following interactions,[2]

$$\gamma_\mu H_5^+ H_5^{+*}: ie(p_+ - p_{+*})_\mu, \quad (16)$$

$$\gamma_\mu H_5^{++} H_5^{+++}: 2ie(p_{++} - p_{+++})_\mu, \quad (17)$$

$$Z_\mu H_5^+ H_5^{+*}: \frac{ie}{2 s_W c_W}(1 - 2s_W^2)(p_+ - p_{+*})_\mu, \quad (18)$$

$$Z_\mu H_5^{++} H_5^{+++}: \frac{ie}{s_W c_W}(1 - 2s_W^2)(p_{++} - p_{+++})_\mu, \quad (19)$$

$$W_\mu^+ H_5^{+*} H_5^0: \frac{\sqrt{3} ie}{2 s_W}(p_{+*} - p_0)_\mu, \quad (20)$$

$$W_\mu^+ H_5^+ H_5^{+++}: \frac{ie}{\sqrt{2} s_W}(p_+ - p_{+++})_\mu, \quad (21)$$

where all fields are incoming and in each case p_Q is the incoming momentum of the scalar with charge Q. Note that these are independent of the mixing angle s_H.

There are theoretical constraints on the Georgi-Machacek model from considerations of perturbativity and vacuum stability [7,13,21], as well as indirect experimental constraints from the measurements of oblique parameters (S, T, U), Z-pole observables (R_b), and B-meson observables [6,13–15,19,25]. Currently the strongest of the indirect experimental bounds arises from measurements of $b \to s\gamma$, which constrain the triplet vev $v_\chi \leq 65$ GeV ($s_H \leq 0.75$) [25]. Additionally, the ATLAS like-sign $WWjj$ cross section measurement, reinterpreted in the context of the GM model in Ref. [23], excludes a doubly charged Higgs $H_5^{\pm\pm}$ with masses in the range $140 \leq m_5 \leq 400$ GeV at $s_H = 0.5$, and $100 \leq m_5 \leq 700$ GeV at $s_H = 1$, under the assumption of a 100% branching fraction for $H_5^{++} \to W^+W^+$. An ATLAS search for singly charged scalars in the VBF production channel similarly excludes $240 \leq m_5 \leq 700$ GeV for $s_H = 1$ under the assumption of a 100% branching fraction for $H_5^+ \to W^+Z$ [44]. Additional constraints on v_χ as a function of the BSM Higgs masses have been obtained in Ref. [26] using ATLAS data from several search channels.

For the simulations that follow, we consider a single benchmark point in the GM model, generated using the calculator GMCALC [37].[3] This point is allowed by all the constraints discussed above. We use the following values for the scalar masses, mixing angles, and additional parameters $M_{1,2}$ as inputs:

[2]As we consider only the fiveplet states in this work, we quote only the relevant interactions involving H_5 scalar states and gauge bosons. A full set of Feynman rules for the GM scalar couplings may be found in Ref. [21].

[3]Our benchmark point corresponds to the default point in GMCALC. The choice of masses, mixing angles, and $M_{1,2}$ as input parameters corresponds to the GMCALC input set 3.

$$m_h = 125\ \text{GeV}, \qquad \sin\alpha = -0.303,$$
$$m_H = 288\ \text{GeV}, \qquad \sin\theta_H = 0.194,$$
$$m_3 = 304\ \text{GeV}, \qquad M_1 = 100\ \text{GeV},$$
$$m_5 = 340\ \text{GeV}, \qquad M_2 = 100\ \text{GeV}. \tag{22}$$

The parameters $M_{1,2}$ are dimensionful parameters in the scalar potential [see Eq. (A1)] that affect the values of the couplings between scalars. The corresponding values for the underlying parameters of the scalar potential are given in Appendix A. While we specify the complete parameter set, note that all the H_5VV couplings are proportional to s_H. Therefore, both the VBF and VH_5 production cross sections of the H_5 states depend only on two parameters, s_H and m_5, and the H_5H_5 production cross sections depend only on m_5. At this parameter point the total widths of the H_5 states are about 0.3 GeV; therefore in our simulations we will take the final-state H_5 particle(s) to be produced on shell.

Finally, we choose the following set of SM inputs:

$$M_W = 80.399\ \text{GeV}, \qquad M_Z = 91.188\ \text{GeV},$$
$$\Gamma_W = 2.085\ \text{GeV}, \qquad \Gamma_Z = 2.495\ \text{GeV},$$
$$G_F = 1.166 \times 10^{-5}\ \text{GeV}^{-2}. \tag{23}$$

$\alpha_{\text{EM}} = 1/132.35$ is computed at tree level from M_W, M_Z, and G_F.

III. COMPUTATIONAL FRAMEWORK

In this work we take advantage of a fully automated framework developed to study the phenomenology of BSM processes at NLO accuracy in QCD, including the matching to parton shower (PS). The framework is based on MadGraph5_aMC@NLO [36]. In order to generate a code capable of computing NLO corrections to a BSM process, some extra information has to be provided besides the usual tree-level Feynman rules. This extra information involves the UV renormalization counterterms and a subset of the rational terms that are needed in the numerical reduction of virtual matrix elements (which are normally referred to as the R_2 terms) [45]. The calculation of the UV and R_2 terms starting from the model Lagrangian has been automatized via the NLOCT package [46], based on FeynRules [35] and FeynArts [47]. Once the UV and R_2 Feynman rules have been generated, they are exported together with the tree-level Feynman rules as a Python module in the Universal FeynRules Output (UFO) format [48]. The Python module can be loaded by any matrix-element generator, such as MadGraph5_aMC@NLO. When the code for the process is written, the UFO information is translated into helicity routines [49] by ALOHA [50]. MadGraph5_aMC@NLO is a metacode that automatically generates the code to perform the simulation of any process up to NLO accuracy in QCD. The simulation can be performed either at fixed order or by generating event samples which can be passed to PS. The automation of the NLO QCD corrections has been achieved by exploiting the FKS [51,52] subtraction scheme to subtract the infrared singularities of real-emission matrix elements, as automated in MadFKS [53]. Loops are computed by MadLoop [54], which exploits the OPP [55] method as well as Tensor Integral Reduction [56,57]; these are implemented in CutTools [58] and IREGI [59], respectively, which are supplemented by an in-house implementation of OpenLoops [60]. Finally, the event generation and matching to PS is done following the MC@NLO procedure [61]. Matching to Herwig6 [62], Pythia6 [63],[4] Herwig++ [64], and Pythia8 [65] is available.

As a consequence, the only input needed to simulate processes in the GM model is the implementation of the model in FeynRules. We have validated our framework by comparing total cross sections at NLO for VBF with the results of the VBF@NNLO code [43,66,67] and found agreement within the integration uncertainties.

IV. VBF PRODUCTION

In the SM, VBF production has been calculated to a rather high level of accuracy: QCD corrections are known up to next-to-next-to-leading order (NNLO) for the total cross section [43,66,68] and for differential observables at the parton level [69–71]. The QCD corrections to the fully inclusive cross sections are fairly moderate, at the level of a few percent. However, the corrections to differential observables are more significant, with NNLO corrections reaching 5%–10% relative to the NLO rate. At both the inclusive and differential levels, the computation of NNLO corrections relies on the so-called structure-function approach [68], which neglects color- and kinematically-suppressed contributions [43,72–75] arising, for example, from the exchange of gluons between the two quark lines. Results at NLO in QCD including parton shower matching have been computed in Refs. [76,77], where it has been found that the typical effect of the shower is to improve the description of jet-related observables by including the effect of extra radiation. NLO electroweak corrections are also known [78,79] and are found to be comparable in size to the NLO QCD ones.

The situation is less satisfactory for BSM scenarios like the Georgi-Machacek model. Although the total cross section can be computed up to NNLO accuracy in QCD [66,67,80], no fully differential prediction exists beyond leading order (LO). As seen in the SM case, corrections to the inclusive total cross sections do not fully capture the behavior at the differential level. In this section we aim to improve this situation, by presenting for the first time fully

[4]Ordered in virtuality or in transverse momentum, with the latter only for processes with no light partons in the final state.

differential results at NLO in QCD including matching to the parton shower.

A. Simulation

The code for VBF production of a fiveplet state in the GM model can be generated and executed in MadGraph5_aMC@NLO with the commands

```
> import model GM_UFO
> generate p p > H5p j j $$ w+ w- z [QCD]
> output VBF_h5p_NLO
> launch
```

Note that we veto W and Z bosons in the s-channel with the \$\$ syntax. The example above generates the code for H_5^+ production. For the other states, H_5^{--}, H_5^-, H_5^0, H_5^{++}, the code can be generated by replacing the `H5p` label with `H5pp~`, `H5p~`, `H5z`, `H5pp`, respectively.

We present results for VBF in the GM model at the LHC Run II energy ($\sqrt{s} = 13$ TeV) at LO and NLO accuracy, in both cases matched to Pythia8. We use the NNPDF 2.3 LO1 and NLO parton density function (PDF) sets [81] consistently with the order of the computation. We keep the renormalization and factorization scales fixed to the W boson mass, as the typical transverse momentum of the tagging jets is of the same order of magnitude. To obtain the uncertainty due to scale variations, we vary the renormalization and factorization scales independently in the range

$$M_W/2 \leq \mu_R, \mu_F \leq 2M_W. \tag{24}$$

We recall that the computation of scale and PDF uncertainties in MadGraph5_aMC@NLO can be performed without the need of extra runs using the reweighting technique presented in Ref. [82]. We employ FastJet [83,84] to cluster hadrons into jets, using the anti-k_T algorithm [85] with a radius parameter $\Delta R = 0.4$. A minimum jet p_T of 30 GeV is required.

In addition, we consider the effect of typical selection cuts used in VBF analyses. These *VBF cuts* require that there are at least two jets and that the two hardest jets satisfy the conditions

$$\begin{aligned} y_j &< 4.5, \\ |y_{j_1} - y_{j_2}| &> 4.0, \\ m(j_1, j_2) &> 600 \text{ GeV}, \end{aligned} \tag{25}$$

where y_j is the jet rapidity and $m(j_1, j_2)$ is the invariant mass of the two jets.

B. Results

In Tables I and II we present the cross sections at the inclusive level and with the VBF cuts of Eq. (25), respectively, for the production via VBF of each of the fiveplet states. Results are shown at LO + PS and NLO + PS, together with the fractional uncertainties obtained from scale variations. First, we note that the K-factors without and with cuts are rather similar to each other. Furthermore, the K-factors for the different fiveplet states are also rather similar and lie around 1.1. The production of more negatively charged Higgs bosons receives slightly larger QCD corrections; this effect, related to the cross section's sensitivity to valence vs sea quarks, becomes slightly more pronounced when VBF cuts are applied. The inclusion of NLO corrections also has the effect of reducing the scale uncertainties to the 1%–2% level. The different dependence on the initial-state quarks of the various processes is also reflected in the efficiency of the VBF cuts. The fraction of events that survives the VBF cuts (tabulated under "cut efficiency" in Table II) varies from 44% in the case of H_5^{--} production to 47% in the case of H_5^{++} production and is essentially unaffected by inclusion of the NLO corrections.

We turn now to study the effect of NLO corrections on differential observables, focusing on the representative case of H_5^+ production in VBF. In Fig. 1, we show the LO + PS and NLO + PS distributions for a number of observables. In particular we consider the transverse momentum p_T and pseudorapidity η of the Higgs boson (H_5) and of the hardest jet (j_1), as well as the invariant mass $m(j_1, j_2)$ and azimuthal separation $\Delta\phi(j_1, j_2)$ of the two hardest jets. The shaded bands show the scale uncertainties at both LO and NLO. The VBF cuts of Eq. (25) have been applied. For each observable, we also show in the inset the differential

TABLE I. Cross sections and K-factors for H_5 VBF production, with scale uncertainties.

Process	LO (fb)	NLO (fb)	K
$pp \to H_5^{--}jj$	$14.94^{+5.4\%}_{-5.1\%}$	$16.72^{+1.4\%}_{-0.7\%}$	1.12
$pp \to H_5^{-}jj$	$16.94^{+5.3\%}_{-5.0\%}$	$18.66^{+1.3\%}_{-0.5\%}$	1.10
$pp \to H_5^{0}jj$	$21.08^{+5.4\%}_{-5.0\%}$	$22.89^{+1.4\%}_{-0.5\%}$	1.09
$pp \to H_5^{+}jj$	$28.07^{+5.8\%}_{-5.3\%}$	$30.14^{+1.5\%}_{-0.7\%}$	1.07
$pp \to H_5^{++}jj$	$40.90^{+6.6\%}_{-5.9\%}$	$43.56^{+1.4\%}_{-0.6\%}$	1.07

TABLE II. Cross sections and K-factors for H_5 VBF production, with scale uncertainties, after applying the VBF cuts given in Eq. (25). Also shown is the fraction of NLO events that survive the VBF cuts (cut efficiency).

Process	LO (fb)	NLO (fb)	K	Cut efficiency
$pp \to H_5^{--}jj$	$6.58^{+7.1\%}_{-6.5\%}$	$7.47^{+1.3\%}_{-1.2\%}$	1.13	0.44
$pp \to H_5^{-}jj$	$7.75^{+7.0\%}_{-6.4\%}$	$8.66^{+1.2\%}_{-0.9\%}$	1.12	0.46
$pp \to H_5^{0}jj$	$9.82^{+7.1\%}_{-6.4\%}$	$10.71^{+1.2\%}_{-0.7\%}$	1.09	0.47
$pp \to H_5^{+}jj$	$13.29^{+7.3\%}_{-6.5\%}$	$14.26^{+1.4\%}_{-0.8\%}$	1.07	0.47
$pp \to H_5^{++}jj$	$19.36^{+7.9\%}_{-7.0\%}$	$20.49^{+1.2\%}_{-0.6\%}$	1.06	0.47

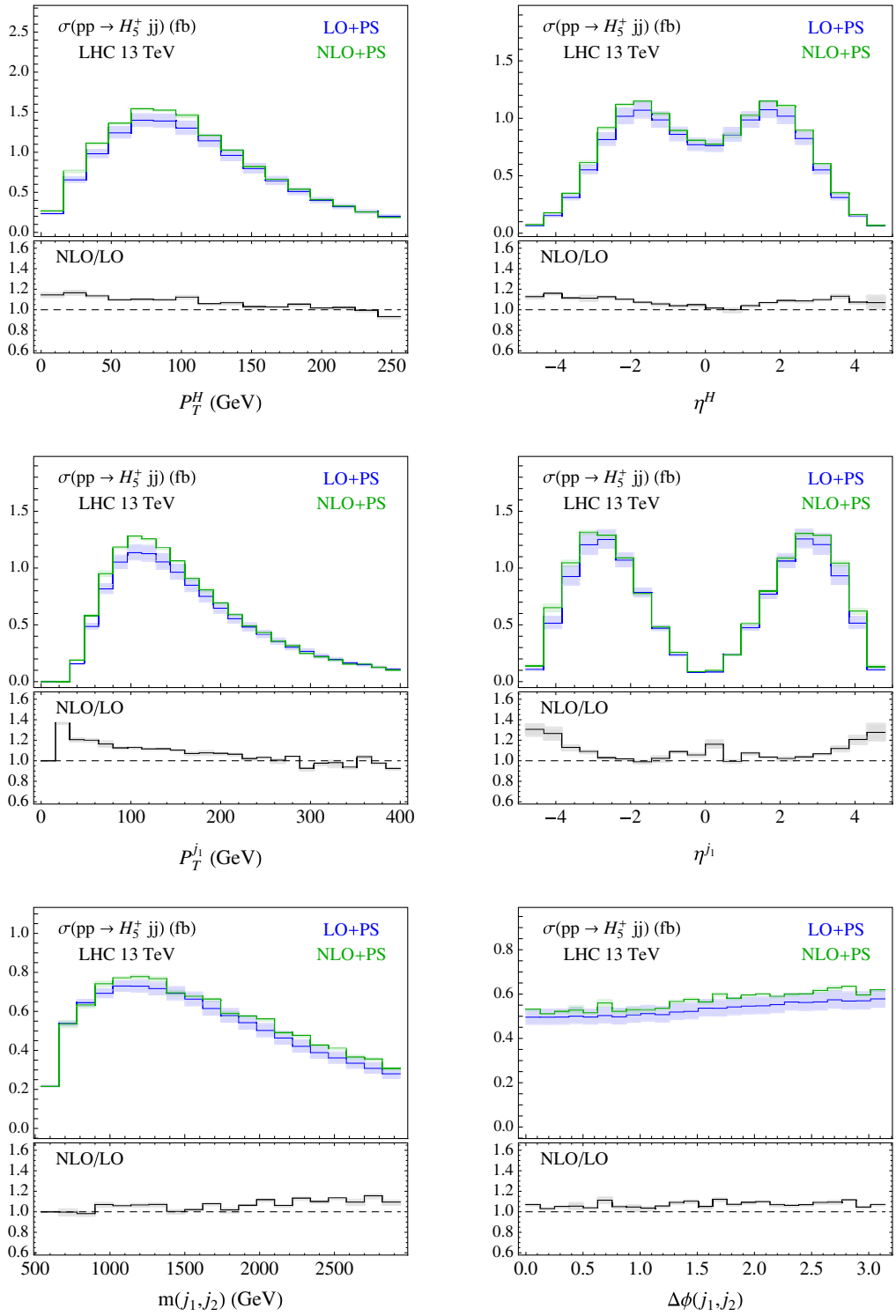

FIG. 1. Differential distributions for VBF production of the H_5^+ boson, with the VBF cuts of Eq. (25) (see the text for details). The distributions for other H_5 states are very similar, differing primarily in overall normalization.

K-factor: that is, the bin-by-bin ratio of the NLO prediction over the LO central value, with the shaded band reflecting the NLO scale uncertainty. As in the case of SM VBF Higgs boson production, the K-factor is in general not constant over the differential distributions. This effect is most visible for the hardest-jet observables. Therefore, a fully differential computation at NLO + PS is strongly preferable to ensure realistic signal simulations.

V. VH_5 PRODUCTION

We now consider the associated production of a GM fiveplet state together with a $W^\pm$ or Z boson. In the SM, the associated production of a Higgs boson with a vector boson is known to NNLO in QCD for the total cross section [86–93]; the two-loop corrections increase the inclusive cross section by less than 5% at the LHC [87]. The QCD corrections to the differential observables are also known to NNLO [94,95], leading to increases of 5%–20% in comparison with the NLO results. N^{3}LO threshold corrections of about 0.1% have also been calculated in Ref. [96]. These results have been implemented along with the electroweak corrections [97,98] in the VH@NNLO code [99].

In the following sections, we present rates and distributions for VH_5 production at NLO for the Georgi-Machacek model.

A. Simulation

The code for associated production of a fiveplet state in the GM model (in this example H_5^+) and a SM vector boson (W^- or Z, decaying leptonically with $l = e$ or μ) can be generated and executed in MadGraph5_aMC@NLO with the commands

```
> import model GM_UFO
> add process p p > H5p l- vl~ [QCD]
> add process p p > H5p l+ l- [QCD]
> output VH_h5p_NLO
> launch
```

In this case, we include the leptonic decay of the gauge bosons at the matrix-element level, so that spin correlations and off-shell effects are automatically taken into account. As in the VBF case, the extension to the other states in the Higgs fiveplet is straightforward. We set the renormalization and factorization scales to the invariant mass of the (reconstructed) VH_5 system, $\mu_R = \mu_F = M_{VH}$.

We consider two sets of cuts. In the first case, we require only basic cuts on leptons and missing transverse energy. Leptons are required to satisfy the transverse momentum and pseudorapidity cuts

$$p_T^l > 30 \text{ GeV} \quad \text{and} \quad \eta_l < 2.5. \tag{26}$$

For WH_5 associated production, we also cut on the transverse missing energy, reconstructed from neutrinos in the event record:

$$E_T^{\text{miss}} > 30 \text{ GeV}. \tag{27}$$

In the second case, we consider a boosted regime, which is often used to enhance the signal-to-background ratio in SM VH searches [100,101], by requiring the following additional cuts on the Higgs and the reconstructed gauge bosons' transverse momenta,

$$p_T^H > 200 \text{ GeV} \quad \text{and} \quad p_T^V > 190 \text{ GeV}, \tag{28}$$

as suggested in Ref. [102].

TABLE III. Cross sections and K-factors for VH_5 production after the basic lepton identification cuts given in Eqs. (26) and (27), with scale uncertainties. For the first three processes the Higgs is produced in association with a Z boson, and for the remainder with a W boson.

Process	LO (fb)	NLO (fb)	K
$pp \to H_5^- l^+ l^-$	$0.01701^{+7.0\%}_{-6.4\%}$	$0.02294^{+1.2\%}_{-0.9\%}$	1.35
$pp \to H_5^0 l^+ l^-$	$0.03570^{+7.1\%}_{-6.4\%}$	$0.04736^{+1.2\%}_{-0.7\%}$	1.33
$pp \to H_5^+ l^+ l^-$	$0.03338^{+7.3\%}_{-6.5\%}$	$0.04332^{+1.4\%}_{-0.8\%}$	1.30
$pp \to H_5^{--} l^+ \nu_l$	$0.10852^{+7.1\%}_{-6.5\%}$	$0.14668^{+1.3\%}_{-1.2\%}$	1.35
$pp \to H_5^- l^+ \nu_l$	$0.08573^{+7.0\%}_{-6.4\%}$	$0.11394^{+1.2\%}_{-0.9\%}$	1.33
$pp \to H_5^0 l^\pm \nu_l^{(-)}$	$0.05354^{+7.1\%}_{-6.4\%}$	$0.07053^{+1.2\%}_{-0.7\%}$	1.32
$pp \to H_5^+ l^- \bar{\nu}_l$	$0.08438^{+7.3\%}_{-6.5\%}$	$0.11192^{+1.4\%}_{-0.8\%}$	1.33
$pp \to H_5^{++} l^- \bar{\nu}_l$	$0.21096^{+7.9\%}_{-7.0\%}$	$0.27332^{+1.2\%}_{-0.6\%}$	1.30

B. Results

In Tables III and IV, we show the cross sections for VH_5 production of H_5 states at LO + PS and NLO + PS with basic cuts and with the additional boosted-regime cuts, respectively. The cross sections include the leptonic branching fractions of the gauge bosons. Note that $ZH_5^{\pm\pm}$ production of the doubly charged states is forbidden by charge conservation. We find that the K-factors are larger than for VBF and, similar to the SM case, lie around

TABLE IV. Cross sections and K-factors for VH_5 production after applying the additional boosted-regime cuts given in Eq. (28). Also shown is the fraction of NLO events that survive the boosted-regime cuts (cut efficiency).

Process	LO (fb)	NLO (fb)	K	Cut efficiency
$pp \to H_5^- l^+ l^-$	$0.00741^{+7.0\%}_{-6.4\%}$	$0.00989^{+1.2\%}_{-0.9\%}$	1.34	0.43
$pp \to H_5^0 l^+ l^-$	$0.01601^{+7.1\%}_{-6.4\%}$	$0.02112^{+1.2\%}_{-0.7\%}$	1.32	0.45
$pp \to H_5^+ l^+ l^-$	$0.01549^{+7.3\%}_{-6.5\%}$	$0.02011^{+1.4\%}_{-0.8\%}$	1.30	0.46
$pp \to H_5^{--} l^+ \nu_l$	$0.04803^{+7.1\%}_{-6.5\%}$	$0.06515^{+1.3\%}_{-1.2\%}$	1.36	0.44
$pp \to H_5^- l^+ \nu_l$	$0.03921^{+7.0\%}_{-6.4\%}$	$0.05188^{+1.2\%}_{-0.9\%}$	1.32	0.46
$pp \to H_5^0 l^\pm \nu_l^{(-)}$	$0.02497^{+7.1\%}_{-6.4\%}$	$0.03278^{+1.2\%}_{-0.7\%}$	1.31	0.46
$pp \to H_5^+ l^- \bar{\nu}_l$	$0.03897^{+7.3\%}_{-6.5\%}$	$0.05163^{+1.4\%}_{-0.8\%}$	1.32	0.46
$pp \to H_5^{++} l^- \bar{\nu}_l$	$0.10158^{+7.9\%}_{-7.0\%}$	$0.13148^{+1.2\%}_{-0.6\%}$	1.29	0.48

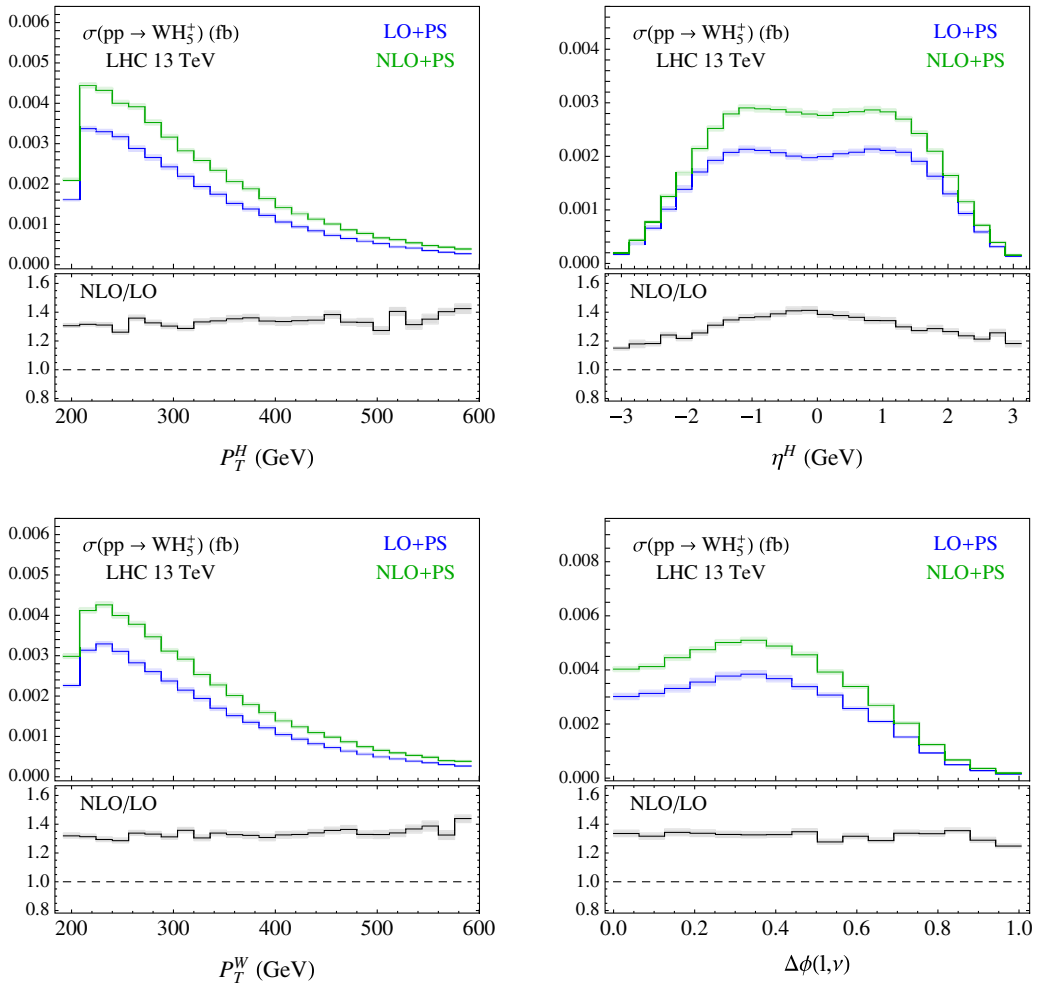

FIG. 2. Differential distributions for WH_5^+ associated production, with the cuts in Eq. (28). The distributions for other H_5 states or for associated production with a Z boson are very similar, differing primarily in overall normalization.

1.3. Furthermore, the value of K-factors without and with the boosted-regime cuts of Eq. (28) are essentially identical. We notice that processes with a more negatively charged final state (which are therefore more sensitive to sea quarks) have slightly larger K-factors. As in the case of VBF, processes with a more positively charged final state have a larger fraction of events which survive the cuts.

In Fig. 2, we present the LO + PS and NLO + PS distributions and K-factors for $W^-H_5^+$ production under the boosted-regime VH_5 cuts given in Eq. (28); the distributions for ZH_5^+ production are similar in shape. We show the transverse momentum p_T and pseudorapidity η of the Higgs, the transverse momentum of the reconstructed vector boson (using Monte Carlo truth information) and the azimuthal separation $\Delta\phi$ between the lepton and the neutrino. In this case we find that the differential K-factors are generally constant over the distributions considered, with the exception of the Higgs pseudorapidity; in this case the K-factor has a maximum of around 1.4 in the central region, which reduces to a minimum of around 1.2 for a Higgs produced in the forward or backward regions.

VI. H_5H_5 PRODUCTION

Finally we consider double Higgs production of two H_5 states in the GM model. In contrast to the SM, pair production of the fiveplet scalars is generally dominated by Drell-Yan-like processes.[5] The exception is $H_5^0H_5^0$ pair production (which we therefore do not consider below), as there is no $ZH_5^0H_5^0$ vertex due to the same symmetry considerations that forbid the ZHH coupling in the SM. $H_5^0H_5^0$ pairs could be produced through VBF, and the

[5]In the SM, Higgs pair production is dominated by gluon fusion at the LHC. The rate of this production mode is known to be quite small and receives important QCD corrections at NLO [103–106]. Corrections to the inclusive cross section have been obtained at NNLO [107–109], while corrections to differential observables are known at NLO [110]. The NNLO corrections to the inclusive cross section are quite large, on the order of 20% [108] in comparison to the NLO result at 14 TeV. The effect of dimension-6 operators arising from new physics has also been considered at NLO in Ref. [111], which found that the new couplings could alter the K-factors relevant to SM-like Higgs pair production by a few percent.

$H_5^0 H_5^0$, $H_5^+ H_5^-$, and $H_5^{++} H_5^{--}$ final states could also be produced via gluon fusion through an off-shell h or H. These processes have very small cross sections and are not considered here.

A. Simulation

The code for the pair production of two fiveplet states in the GM model, for example $H_5^{--} H_5^+$, can be generated and executed in MADGRAPH5_AMC@NLO with the commands

```
> import model GM_UFO
> generate p p > H5pp~ H5p [QCD]
> output H5mm_H5p_NLO
> launch
```

Once again, the extension to the other combinations of states in the Higgs fiveplet is straightforward. We set the renormalization and factorization scales to the invariant mass of the Higgs pair, $\mu_R = \mu_F = M_{HH}$. We do not consider additional cuts on these processes.

TABLE V. Cross sections and K-factors for $H_5 H_5$ production, with scale uncertainties. The first two processes proceed through an s-channel W^-, the next two through a Z, and the last two through a W^+.

Process	LO (fb)	NLO (fb)	K
$pp \to H_5^{--} H_5^+$	$2.113^{+4.4\%}_{-4.2\%}$	$2.977^{+2.2\%}_{-2.1\%}$	1.41
$pp \to H_5^- H_5^0$	$3.174^{+4.4\%}_{-4.2\%}$	$4.464^{+2.2\%}_{-2.1\%}$	1.41
$pp \to H_5^{--} H_5^{++}$	$7.589^{+4.4\%}_{-4.2\%}$	$10.499^{+2.2\%}_{-2.1\%}$	1.38
$pp \to H_5^- H_5^+$	$1.897^{+4.4\%}_{-4.2\%}$	$2.624^{+2.2\%}_{-2.1\%}$	1.38
$pp \to H_5^0 H_5^+$	$7.128^{+4.6\%}_{-4.4\%}$	$9.671^{+2.2\%}_{-2.2\%}$	1.36
$pp \to H_5^- H_5^{++}$	$4.752^{+4.6\%}_{-4.4\%}$	$6.448^{+2.2\%}_{-2.2\%}$	1.36

B. Results

In Table V we show the cross sections for $H_5 H_5$ production at LO + PS and NLO + PS, without cuts. In Fig. 3, we show the LO + PS and NLO + PS distributions and K-factors for $H_5^{--} H_5^+$ production. We show the transverse momentum p_T and pseudorapidity η of the scalar

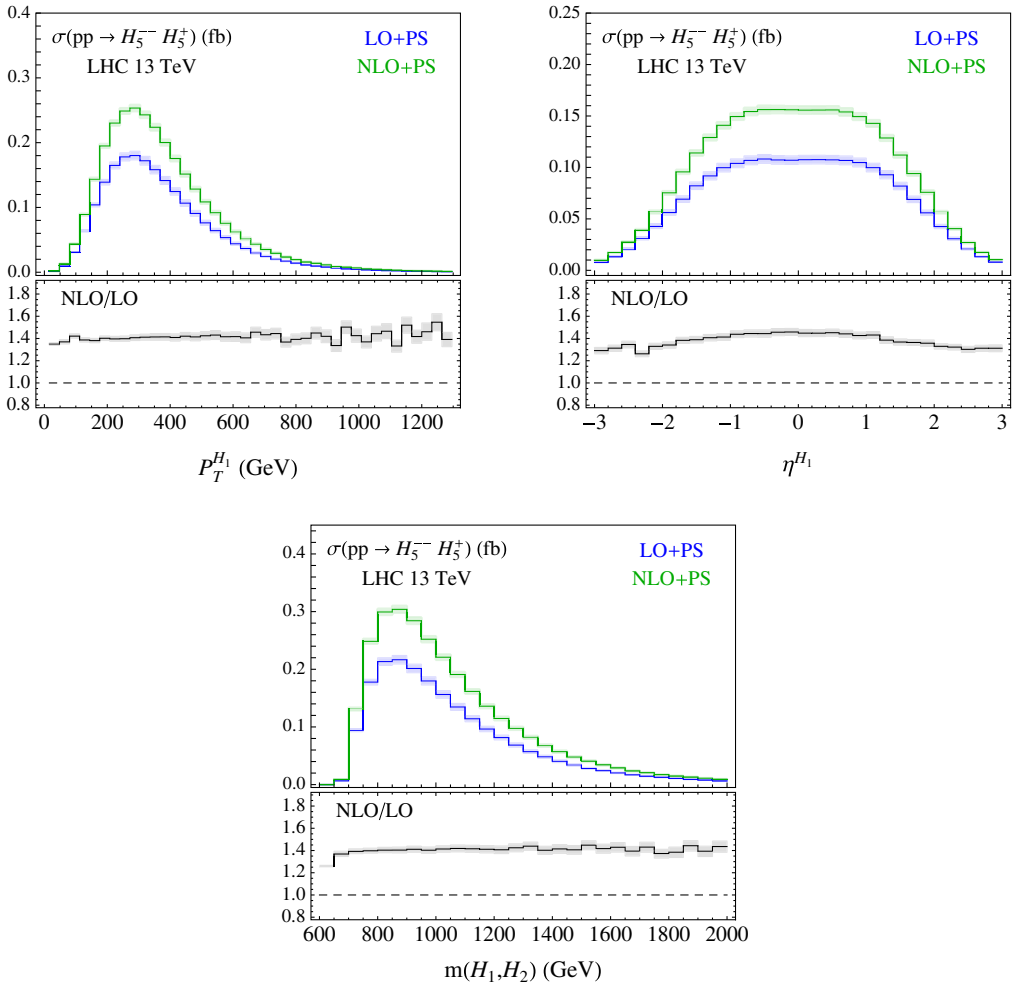

FIG. 3. Differential distributions for $H_5^{--} H_5^+$ associated production. The distributions for other H_5 states are very similar, differing primarily in overall normalization.

H_5^{--} and the invariant mass of the two scalars. The p_T and η distributions of the other scalar H_5^+ are similar.

As in the case of VH_5 production, the differential K-factors are generally constant over the distributions considered, with the exception of the Higgs pseudorapidities; in this case the K-factor has a maximum slightly above 1.4 in the central region, which reduces to roughly 1.3 for a Higgs produced in the forward or backward regions.

VII. CONCLUSIONS

We have presented cross sections, differential distributions, and K-factors for the production of fermiophobic fiveplet scalars in the Georgi-Machacek model at NLO accuracy in QCD, including the matching to parton showers. We considered production through VBF, VH_5, and H_5H_5 associated production at the benchmark point of Eq. (22). Our results demonstrate the importance of a fully differential simulation at NLO + PS in order to accurately simulate the signal at the LHC. Automated tools make such a simulation possible with a very limited effort. For what concerns VH_5 and H_5H_5 production, the description of the final state can be further improved by including the effect of the radiation of extra jets at NLO accuracy, for example using the Fx-Fx [112] or UNLOPS [113] merging technique, which are both automatized within MadGraph5_aMC@NLO. The model files for the automated tool chain used to produce these results are publicly available on http://feynrules.irmp.ucl.ac.be/wiki/GeorgiMachacekModel.

ACKNOWLEDGMENTS

We thank K. Kumar for helpful discussions about the Georgi-Machacek model and FeynRules, and we are grateful to F. Maltoni and L. Barak for having encouraged us to pursue the present project. C. D. is a Durham International Junior Research Fellow and has been supported in part by the Research Executive Agency of the European Union under Grant No. PITN-GA-2012-315877 (MC-Net). K. H., H. E. L., and A. P. were supported by the Natural Sciences and Engineering Research Council of Canada. K. H. was also supported by the Government of Ontario through an Ontario Graduate Scholarship. M. Z. is supported by the European Union's Horizon 2020 research and innovation program under the Marie Sklodovska-Curie Grant No. 660171 and in part by the ERC grant Higgs@LHC and by the ILP LABEX (reference ANR-10-LABX-63), in turn supported by French state funds managed by the ANR within the "Investissements d'Avenir" programme under reference ANR-11-IDEX-0004-02.

APPENDIX: THE SCALAR POTENTIAL AND MASSES OF THE GEORGI-MACHACEK MODEL

The most general gauge-invariant scalar potential involving these fields that conserves custodial $SU(2)$ can be written as[6] [21]

$$\begin{aligned} V(\Phi, X) = {} & \frac{\mu_2^2}{2}\mathrm{Tr}(\Phi^\dagger\Phi) + \frac{\mu_3^2}{2}\mathrm{Tr}(X^\dagger X) + \lambda_1[\mathrm{Tr}(\Phi^\dagger\Phi)]^2 + \lambda_2\mathrm{Tr}(\Phi^\dagger\Phi)\mathrm{Tr}(X^\dagger X) \\ & + \lambda_3\mathrm{Tr}(X^\dagger X X^\dagger X) + \lambda_4[\mathrm{Tr}(X^\dagger X)]^2 - \lambda_5\mathrm{Tr}(\Phi^\dagger\tau^a\Phi\tau^b)\mathrm{Tr}(X^\dagger t^a X t^b) \\ & - M_1\mathrm{Tr}(\Phi^\dagger\tau^a\Phi\tau^b)(UXU^\dagger)_{ab} - M_2\mathrm{Tr}(X^\dagger t^a X t^b)(UXU^\dagger)_{ab}. \end{aligned} \tag{A1}$$

Here the $SU(2)$ generators for the doublet representation are $\tau^a = \sigma^a/2$ with σ^a being the Pauli matrices; the generators for the triplet representation are

$$t^1 = \frac{1}{\sqrt{2}}\begin{pmatrix} 0 & 1 & 0 \\ 1 & 0 & 1 \\ 0 & 1 & 0 \end{pmatrix}, \qquad t^2 = \frac{1}{\sqrt{2}}\begin{pmatrix} 0 & -i & 0 \\ i & 0 & -i \\ 0 & i & 0 \end{pmatrix},$$
$$t^3 = \begin{pmatrix} 1 & 0 & 0 \\ 0 & 0 & 0 \\ 0 & 0 & -1 \end{pmatrix}; \tag{A2}$$

and the matrix U, which rotates X into the Cartesian basis, is given by [7]

$$U = \begin{pmatrix} -\frac{1}{\sqrt{2}} & 0 & \frac{1}{\sqrt{2}} \\ -\frac{i}{\sqrt{2}} & 0 & -\frac{i}{\sqrt{2}} \\ 0 & 1 & 0 \end{pmatrix}. \tag{A3}$$

In the notation of the parameters of the scalar potential, our chosen benchmark point corresponds to values of

$$\begin{aligned} &\mu_2^2 = -(92.0\ \mathrm{GeV})^2, \qquad \lambda_2 = \lambda_3 = \lambda_4 = \lambda_5 = 0.1, \\ &\mu_3^2 = (300\ \mathrm{GeV})^2, \qquad M_1 = M_2 = 100\ \mathrm{GeV}. \\ &\lambda_1 = 0.0468, \end{aligned} \tag{A4}$$

Here μ_2^2 and λ_1 have, respectively, been set using G_F and $m_h = 125$ GeV [see Eq. (A11)].

The vevs are obtained by solving the minimization conditions,

[6] A translation table to other parametrizations in the literature has been given in an Appendix of Ref. [21]. Note that Refs. [3–6,8,11,12,15,17,18,20] impose an additional Z_2 symmetry on this potential, such that $M_1 = M_2 = 0$ and the model has no decoupling limit.

$$v_\phi\left[\mu_2^2+4\lambda_1 v_\phi^2+3(2\lambda_2-\lambda_5)v_\chi^2-\frac{3}{2}M_1 v_\chi\right]=0,$$
$$3\mu_3^2 v_\chi+3(2\lambda_2-\lambda_5)v_\phi^2 v_\chi+12(\lambda_3+3\lambda_4)v_\chi^3 -\frac{3}{4}M_1 v_\phi^2-18M_2 v_\chi^2=0. \quad \text{(A5)}$$

After electroweak symmetry breaking, the masses of the custodial fiveplet and triplet scalars are, respectively, given by

$$m_5^2=\frac{M_1}{4v_\chi}v_\phi^2+12M_2 v_\chi+\frac{3}{2}\lambda_5 v_\phi^2+8\lambda_3 v_\chi^2,$$
$$m_3^2=\frac{M_1}{4v_\chi}(v_\phi^2+8v_\chi^2)+\frac{\lambda_5}{2}(v_\phi^2+8v_\chi^2)=\left(\frac{M_1}{4v_\chi}+\frac{\lambda_5}{2}\right)v^2. \quad \text{(A6)}$$

The mixing of the custodial singlets is controlled by the 2×2 mass-squared matrix

$$\mathcal{M}^2=\begin{pmatrix}\mathcal{M}_{11}^2 & \mathcal{M}_{12}^2\\ \mathcal{M}_{12}^2 & \mathcal{M}_{22}^2\end{pmatrix}, \quad \text{(A7)}$$

where

$$\mathcal{M}_{11}^2=8\lambda_1 v_\phi^2,$$
$$\mathcal{M}_{12}^2=\frac{\sqrt{3}}{2}v_\phi[-M_1+4(2\lambda_2-\lambda_5)v_\chi],$$
$$\mathcal{M}_{22}^2=\frac{M_1 v_\phi^2}{4v_\chi}-6M_2 v_\chi+8(\lambda_3+3\lambda_4)v_\chi^2. \quad \text{(A8)}$$

The mixing angle α is then fixed by

$$\sin 2\alpha=\frac{2\mathcal{M}_{12}^2}{m_H^2-m_h^2}, \qquad \cos 2\alpha=\frac{\mathcal{M}_{22}^2-\mathcal{M}_{11}^2}{m_H^2-m_h^2}, \quad \text{(A9)}$$

and the singlet masses are given by

$$m_{h,H}^2=\frac{1}{2}\left[\mathcal{M}_{11}^2+\mathcal{M}_{22}^2\mp\sqrt{(\mathcal{M}_{11}^2-\mathcal{M}_{22}^2)^2+4(\mathcal{M}_{12}^2)^2}\right]. \quad \text{(A10)}$$

The relationship that allows λ_1 to be fixed in terms of the measured mass of the observed SM-like Higgs boson is obtained by inverting Eq. (A10):

$$\lambda_1=\frac{1}{8v_\phi^2}\left[m_h^2+\frac{(\mathcal{M}_{12}^2)^2}{\mathcal{M}_{22}^2-m_h^2}\right]. \quad \text{(A11)}$$

[1] H. Georgi and M. Machacek, Nucl. Phys. **B262**, 463 (1985).
[2] M. S. Chanowitz and M. Golden, Phys. Lett. **165B**, 105 (1985).
[3] J. F. Gunion, R. Vega, and J. Wudka, Phys. Rev. D **43**, 2322 (1991).
[4] J. F. Gunion, R. Vega, and J. Wudka, Phys. Rev. D **42**, 1673 (1990).
[5] A. G. Akeroyd, Phys. Lett. B **442**, 335 (1998).
[6] H. E. Haber and H. E. Logan, Phys. Rev. D **62**, 015011 (2000).
[7] M. Aoki and S. Kanemura, Phys. Rev. D **77**, 095009 (2008); **89**, 059902 (2014).
[8] S. Godfrey and K. Moats, Phys. Rev. D **81**, 075026 (2010).
[9] I. Low and J. Lykken, J. High Energy Phys. 10 (2010) 053.
[10] H. E. Logan and M. A. Roy, Phys. Rev. D **82**, 115011 (2010).
[11] D. Carmi, A. Falkowski, E. Kuflik, T. Volansky, and J. Zupan, J. High Energy Phys. 10 (2012) 196.
[12] S. Chang, C. A. Newby, N. Raj, and C. Wanotayaroj, Phys. Rev. D **86**, 095015 (2012).
[13] C. W. Chiang and K. Yagyu, J. High Energy Phys. 01 (2013) 026.
[14] S. Kanemura, M. Kikuchi, and K. Yagyu, Phys. Rev. D **88**, 015020 (2013).
[15] C. Englert, E. Re, and M. Spannowsky, Phys. Rev. D **87**, 095014 (2013).
[16] R. Killick, K. Kumar, and H. E. Logan, Phys. Rev. D **88**, 033015 (2013).
[17] G. Belanger, B. Dumont, U. Ellwanger, J. F. Gunion, and S. Kraml, Phys. Rev. D **88**, 075008 (2013).
[18] C. Englert, E. Re, and M. Spannowsky, Phys. Rev. D **88**, 035024 (2013).
[19] C. W. Chiang, A. L. Kuo, and K. Yagyu, J. High Energy Phys. 10 (2013) 072.
[20] A. Efrati and Y. Nir, arXiv:1401.0935.
[21] K. Hartling, K. Kumar, and H. E. Logan, Phys. Rev. D **90**, 015007 (2014).
[22] C. W. Chiang and T. Yamada, Phys. Lett. B **735**, 295 (2014).
[23] C. W. Chiang, S. Kanemura, and K. Yagyu, Phys. Rev. D **90**, 115025 (2014).
[24] S. I. Godunov, M. I. Vysotsky, and E. V. Zhemchugov, J. Exp. Theor. Phys. **120**, 369 (2015).
[25] K. Hartling, K. Kumar, and H. E. Logan, Phys. Rev. D **91**, 015013 (2015).
[26] C. W. Chiang and K. Tsumura, J. High Energy Phys. 04 (2015) 113.
[27] S. I. Godunov, M. I. Vysotsky, and E. V. Zhemchugov, Phys. Lett. B **751**, 505 (2015).

[28] C. W. Chiang, S. Kanemura, and K. Yagyu, arXiv: 1510.06297.
[29] S. Chang and J. G. Wacker, Phys. Rev. D **69**, 035002 (2004).
[30] S. Chang, J. High Energy Phys. 12 (2003) 057.
[31] L. Cort, M. Garcia, and M. Quiros, Phys. Rev. D **88**, 075010 (2013).
[32] M. Garcia-Pepin, S. Gori, M. Quiros, R. Vega, R. Vega-Morales, and T. T. Yu, Phys. Rev. D **91**, 015016 (2015).
[33] A. Delgado, M. Garcia-Pepin, and M. Quiros, J. High Energy Phys. 08 (2015) 159.
[34] H. E. Logan and V. Rentala, Phys. Rev. D **92**, 075011 (2015).
[35] A. Alloul, N. D. Christensen, C. Degrande, C. Duhr, and B. Fuks, Comput. Phys. Commun. **185**, 2250 (2014).
[36] J. Alwall, R. Frederix, S. Frixione, V. Hirschi, F. Maltoni, O. Mattelaer, H.-S. Shao, T. Stelzer, P. Torrielli, and M. Zaro, J. High Energy Phys. 07 (2014) 079.
[37] K. Hartling, K. Kumar, and H. E. Logan, arXiv:1412.7387.
[38] J. Beringer *et al.* (Particle Data Group Collaboration), Phys. Rev. D **86**, 010001 (2012).
[39] G. Aad *et al.* (ATLAS Collaboration), Phys. Lett. B **716**, 1 (2012).
[40] S. Chatrchyan *et al.* (CMS Collaboration), Phys. Lett. B **716**, 30 (2012).
[41] G. Aad *et al.* (ATLAS and CMS Collaborations), Phys. Rev. Lett. **114**, 191803 (2015).
[42] J. F. Gunion, H. E. Haber, G. L. Kane, and S. Dawson, *The Higgs Hunter's Guide* (Westview, Boulder, CO, 2000).
[43] P. Bolzoni, F. Maltoni, S. O. Moch, and M. Zaro, Phys. Rev. D **85**, 035002 (2012).
[44] G. Aad *et al.* (ATLAS Collaboration), Phys. Rev. Lett. **114**, 231801 (2015).
[45] G. Ossola, C. G. Papadopoulos, and R. Pittau, J. High Energy Phys. 05 (2008) 004.
[46] C. Degrande, Comput. Phys. Commun. **197**, 239 (2015).
[47] T. Hahn, Comput. Phys. Commun. **140**, 418 (2001).
[48] C. Degrande, C. Duhr, B. Fuks, D. Grellscheid, O. Mattelaer, and T. Reiter, Comput. Phys. Commun. **183**, 1201 (2012).
[49] H. Murayama, I. Watanabe, and K. Hagiwara, Report No. KEK-91-11.
[50] P. de Aquino, W. Link, F. Maltoni, O. Mattelaer, and T. Stelzer, Comput. Phys. Commun. **183**, 2254 (2012).
[51] S. Frixione, Z. Kunszt, and A. Signer, Nucl. Phys. **B467**, 399 (1996).
[52] S. Frixione, Nucl. Phys. **B507**, 295 (1997).
[53] R. Frederix, S. Frixione, F. Maltoni, and T. Stelzer, J. High Energy Phys. 10 (2009) 003.
[54] V. Hirschi, R. Frederix, S. Frixione, M. V. Garzelli, F. Maltoni, and R. Pittau, J. High Energy Phys. 05 (2011) 044.
[55] G. Ossola, C. G. Papadopoulos, and R. Pittau, Nucl. Phys. **B763**, 147 (2007).
[56] G. Passarino and M. J. G. Veltman, Nucl. Phys. **B160**, 151 (1979).
[57] A. I. Davydychev, Phys. Lett. B **263**, 107 (1991).
[58] G. Ossola, C. G. Papadopoulos, and R. Pittau, J. High Energy Phys. 03 (2008) 042.
[59] V. Hirschi and O. Mattelaer, J. High Energy Phys. 10 (2015) 146.
[60] F. Cascioli, P. Maierhofer, and S. Pozzorini, Phys. Rev. Lett. **108**, 111601 (2012).
[61] S. Frixione and B. R. Webber, J. High Energy Phys. 06 (2002) 029.
[62] G. Corcella, I. G. Knowles, G. Marchesini, S. Moretti, K. Odagiri, P. Richardson, M. H. Seymour, and B. R. Webber, J. High Energy Phys. 01 (2001) 010.
[63] T. Sjostrand, S. Mrenna, and P. Z. Skands, J. High Energy Phys. 05 (2006) 026.
[64] M. Bahr *et al.*, Eur. Phys. J. C **58**, 639 (2008).
[65] T. Sjostrand, S. Mrenna, and P. Z. Skands, Comput. Phys. Commun. **178**, 852 (2008).
[66] P. Bolzoni, F. Maltoni, S. O. Moch, and M. Zaro, Phys. Rev. Lett. **105**, 011801 (2010).
[67] M. Zaro, P. Bolzoni, F. Maltoni, and S. O. Moch, *Proc. Sci.* CHARGED2010 (2010) 028.
[68] T. Han, G. Valencia, and S. Willenbrock, Phys. Rev. Lett. **69**, 3274 (1992).
[69] T. Figy, C. Oleari, and D. Zeppenfeld, Phys. Rev. D **68**, 073005 (2003).
[70] K. Arnold *et al.*, Comput. Phys. Commun. **180**, 1661 (2009).
[71] M. Cacciari, F. A. Dreyer, A. Karlberg, G. P. Salam, and G. Zanderighi, Phys. Rev. Lett. **115**, 082002 (2015).
[72] W. L. van Neerven and J. A. M. Vermaseren, Phys. Lett. B **142**, 80 (1984).
[73] J. Blumlein, G. J. van Oldenborgh, and R. Ruckl, Nucl. Phys. **B395**, 35 (1993).
[74] T. Figy, V. Hankele, and D. Zeppenfeld, J. High Energy Phys. 02 (2008) 076.
[75] R. V. Harlander, J. Vollinga, and M. M. Weber, Phys. Rev. D **77**, 053010 (2008).
[76] P. Nason and C. Oleari, J. High Energy Phys. 02 (2010) 037.
[77] S. Frixione, P. Torrielli, and M. Zaro, Phys. Lett. B **726**, 273 (2013).
[78] M. Ciccolini, A. Denner, and S. Dittmaier, Phys. Rev. Lett. **99**, 161803 (2007).
[79] M. Ciccolini, A. Denner, and S. Dittmaier, Phys. Rev. D **77**, 013002 (2008).
[80] M. Zaro and H. Logan, Report No. LHCHXSWG-2015-001.
[81] R. D. Ball *et al.*, Nucl. Phys. **B867**, 244 (2013).
[82] R. Frederix, S. Frixione, V. Hirschi, F. Maltoni, R. Pittau, and P. Torrielli, J. High Energy Phys. 02 (2012) 099.
[83] M. Cacciari and G. P. Salam, Phys. Lett. B **641**, 57 (2006).
[84] M. Cacciari, G. P. Salam, and G. Soyez, Eur. Phys. J. C **72**, 1896 (2012).
[85] M. Cacciari, G. P. Salam, and G. Soyez, J. High Energy Phys. 04 (2008) 063.
[86] T. Han and S. Willenbrock, Phys. Lett. B **273**, 167 (1991).
[87] O. Brein, A. Djouadi, and R. Harlander, Phys. Lett. B **579**, 149 (2004).
[88] J. Ohnemus and W. J. Stirling, Phys. Rev. D **47**, 2722 (1993).
[89] H. Baer, B. Bailey, and J. F. Owens, Phys. Rev. D **47**, 2730 (1993).

[90] O. Brein, R. Harlander, M. Wiesemann, and T. Zirke, Eur. Phys. J. C **72**, 1868 (2012).
[91] B. A. Kniehl, Phys. Rev. D **42**, 2253 (1990).
[92] L. Altenkamp, S. Dittmaier, R. V. Harlander, H. Rzehak, and T. J. E. Zirke, J. High Energy Phys. 02 (2013) 078.
[93] R. V. Harlander, A. Kulesza, V. Theeuwes, and T. Zirke, J. High Energy Phys. 11 (2014) 082.
[94] G. Ferrera, M. Grazzini, and F. Tramontano, Phys. Lett. B **740**, 51 (2015).
[95] G. Ferrera, M. Grazzini, and F. Tramontano, Phys. Rev. Lett. **107**, 152003 (2011).
[96] M. C. Kumar, M. K. Mandal, and V. Ravindran, J. High Energy Phys. 03 (2015) 037.
[97] M. L. Ciccolini, S. Dittmaier, and M. Kramer, Phys. Rev. D **68**, 073003 (2003).
[98] O. Brein, M. Ciccolini, S. Dittmaier, A. Djouadi, R. Harlander, and M. Kramer, arXiv:hep-ph/0402003.
[99] O. Brein, R. V. Harlander, and T. J. E. Zirke, Comput. Phys. Commun. **184**, 998 (2013).
[100] J. M. Butterworth, A. R. Davison, M. Rubin, and G. P. Salam, Phys. Rev. Lett. **100**, 242001 (2008).
[101] ATLAS Collaboration, Report Nos. ATL-PHYS-PUB-2009-088, ATL-COM-PHYS-2009-345.
[102] S. Heinemeyer *et al.* (LHC Higgs Cross Section Working Group Collaboration), arXiv:1307.1347.
[103] T. Plehn, M. Spira, and P. M. Zerwas, Nucl. Phys. **B479**, 46 (1996); **B531**, 655 (1998).
[104] S. Dawson, S. Dittmaier, and M. Spira, Phys. Rev. D **58**, 115012 (1998).
[105] T. Binoth, S. Karg, N. Kauer, and R. Ruckl, Phys. Rev. D **74**, 113008 (2006).
[106] J. Baglio, A. Djouadi, R. Gröber, M. M. Mühlleitner, J. Quevillon, and M. Spira, J. High Energy Phys. 04 (2013) 151.
[107] D. de Florian and J. Mazzitelli, Phys. Lett. B **724**, 306 (2013).
[108] D. de Florian and J. Mazzitelli, Phys. Rev. Lett. **111**, 201801 (2013).
[109] J. Grigo, K. Melnikov, and M. Steinhauser, Nucl. Phys. **B888**, 17 (2014).
[110] R. Frederix, S. Frixione, V. Hirschi, F. Maltoni, O. Mattelaer, P. Torrielli, E. Vryonidou, and M. Zaro, Phys. Lett. B **732**, 142 (2014).
[111] R. Grober, M. Muhlleitner, M. Spira, and J. Streicher, J. High Energy Phys. 09 (2015) 092.
[112] R. Frederix and S. Frixione, J. High Energy Phys. 12 (2012) 061.
[113] L. Lönnblad and S. Prestel, J. High Energy Phys. 03 (2013) 166.